The 2010 M_w 8.8 Maule, Chile earthquake: Nucleation and rupture propagation controlled by a subducted topographic high

Stephen P. Hicks,[1] Andreas Rietbrock,[1] Christian A. Haberland,[2] Isabelle M. A. Ryder,[1] Mark Simons,[3] and Andrés Tassara[4]

Received 24 July 2012; revised 8 September 2012; accepted 14 September 2012; published 13 October 2012.

[1] Knowledge of seismic properties in an earthquake rupture zone is essential for understanding the factors controlling rupture dynamics. We use data from aftershocks following the Maule earthquake to derive a three-dimensional seismic velocity model of the central Chile forearc. At 36°S, we find a high v_p (>7.0 km/s) and high v_p/v_s (∼1.89) anomaly lying along the megathrust at 25 km depth, which coincides with a strong forearc Bouguer gravity signal. We interpret this as a subducted topographic high, possibly a former seamount on the Nazca slab. The Maule earthquake nucleated at the anomaly's updip boundary; yet high co-seismic slip occurred where the megathrust is overlain by lower seismic velocities. Sparse aftershock seismicity occurs within this structure, suggesting that it disrupts normal interface seismogenesis. These findings imply that subducted structures can be conducive to the nucleation of large megathrust earthquakes, even if they subsequently hinder co-seismic slip and aftershock activity. **Citation:** Hicks, S. P., A. Rietbrock, C. A. Haberland, I. M. A. Ryder, M. Simons, and A. Tassara (2012), The 2010 M_w 8.8 Maule, Chile earthquake: Nucleation and rupture propagation controlled by a subducted topographic high, *Geophys. Res. Lett.*, *39*, L19308, doi:10.1029/2012GL053184.

1. Introduction

[2] The rupture dynamics of great subduction zone earthquakes are complex. Due to the vast increase in instrumentation in recent years, geophysicists can now map high-order spatial variations in energy release and seismic slip along the megathrust. However, our understanding of the factors that influence these spatial variations remains limited. The February 2010 M_w 8.8 Maule earthquake, which ruptured an 81,500 km^2 area [*Lay et al.*, 2010] of the subduction interface between the downgoing Nazca and overriding South American plate, is no exception. This segment had not experienced a large rupture since the great 1835 Concepción earthquake (Figure 1a). The 'Darwin gap' [*Lorito et al.*, 2011] was recognised as a mature seismic gap and geodetic measurements acquired before the 2010 event indicated strong locking of the megathrust within the gap [*Ruegg et al.*, 2009; *Moreno et al.*, 2010; *Métois et al.*, 2012]. The earthquake nucleated in the Darwin gap; however, published co-seismic slip models imply bilateral rupture propagation [*Lay et al.*, 2010; *Lorito et al.*, 2011; *Vigny et al.*, 2011; *Moreno et al.*, 2012], with up to 20 m of slip ∼100 km north of the hypocentre, and up to 10 m of slip to the south.

[3] The subduction zone asperity model [*Lay and Kanamori*, 1981] provides a conceptual framework to explain the slip distribution of large earthquakes. According to this model, areas of large co-seismic slip are caused by asperities that are interseismically locked. Studies of strike-slip earthquakes [*Michael and Eberhart-Phillips*, 1991; *Okada et al.*, 2007] suggest that asperities are associated with high seismic velocities, and therefore competent material. For subduction earthquakes, however, topographic highs (e.g. ridges, fracture zones, seamounts) on the subducting plate can act as rupture barriers [*Kodaira et al.*, 2002; *Park et al.*, 2004; *Robinson et al.*, 2006].

[4] Recently-published aftershock distributions [*Lange et al.*, 2012; *Rietbrock et al.*, 2012] for the Maule earthquake show a gap in interface seismicity at 30–40 km depth, prominent near 36°S. The slip models and aftershock patterns demonstrate that spatial heterogeneity exists along the fault. It is therefore important to assess whether any heterogeneity in the rupture zone is expressed in its seismic properties, and whether we can identify any correlation with co-seismic slip. Here, we use travel-time data from aftershocks to reveal a high-velocity anomaly along the megathrust interface in the Darwin gap.

2. Tomographic Inversion Scheme

[5] Following the Maule earthquake, a concerted multinational seismic deployment took place to record aftershock activity. The network consisted of ∼160 stations covering the entire rupture area (Figure 1b). We determine the seismic structure in the rupture area using data from the International Maule Aftershock Dataset (IMAD). We automatically detect seismic P- and S-wave arrival times from aftershocks using an optimised STA/LTA triggering algorithm [*Nippress et al.*, 2009] with an iterative location algorithm [*Rietbrock et al.*, 2012], ensuring data consistency. Picking errors for the automatic analysis are shown in Figure S1 of the auxiliary material.[1]

[6] We use a staggered inversion scheme [e.g., *Haberland et al.*, 2009] to generate the velocity model. We estimate a best-fitting minimum 1D model using the VELEST

[1]School of Environmental Sciences, University of Liverpool, Liverpool, UK.
[2]Deutsches GeoForschungsZentrum, Potsdam, Germany.
[3]Geological and Planetary Sciences, California Institute of Technology, Pasadena, California, USA.
[4]Departamento de Ciencias de la Tierra, Universidad de Concepción, Concepción, Chile.

Corresponding author: S. P. Hicks, School of Environmental Sciences, University of Liverpool, Jane Herdman Laboratories, 4 Brownlow St., Liverpool L69 3GP, UK. (s.hicks@liv.ac.uk)

0094-8276/12/2012GL053184

[1]Auxiliary materials are available in the HTML. doi:10.1029/2012GL053184.

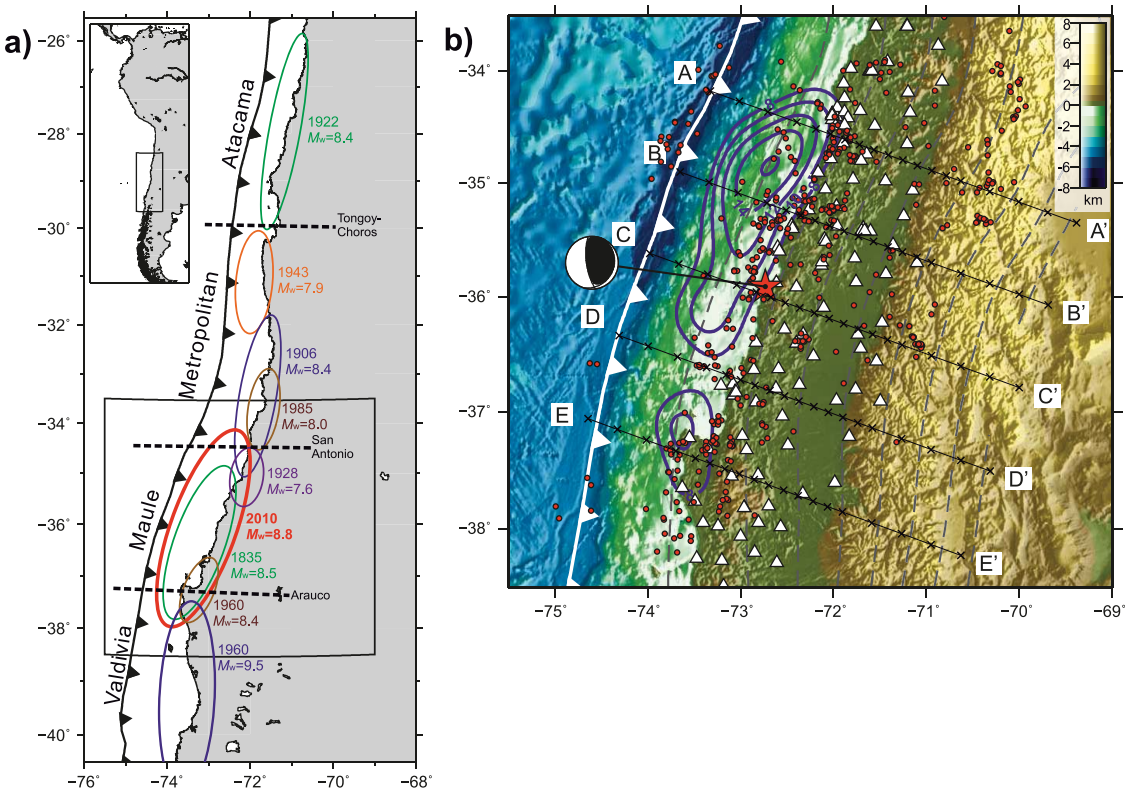

Figure 1. Locations of past ruptures and segmentation in Chile, after *Métois et al.* [2012]; ellipses give the rupture area of each earthquake. The name of each segment and segment boundaries (dashed lines) are shown. The box denotes the location of the map in Figure 1b. (b) Local map with bathymetry/topography (coloured scale bar). The red star is the NEIC epicentre. Blue contour lines show the co-seismic slip distribution of *Moreno et al.* [2012]. Red circles and white triangles are the aftershocks and stations, respectively, used in our tomographic inversion. Black crosses denote the nodes in our 3D inversion. The grey dashed lines show the geometry of the subducting Nazca slab, based on the Slab1.0 model [*Hayes and Wald*, 2009].

algorithm [*Kissling et al.*, 1994]. For the tomographic inversion, we choose 397 events (Figure 1b) from the first two months of aftershocks based on a maximum azimuthal gap criterion (onshore events <175°; offshore events <270°) and the number of S-wave picks (>40). We require a well-distributed aftershock catalogue to ensure good ray coverage in the model. This catalogue yields ~30,000 P-wave and ~19,000 S-wave travel-time observations. We use the SIMUL2000 code [*Thurber*, 1983] to invert for both v_p and v_p/v_s, incorporating a non-uniform nodal spacing (Figure 1b) in the x-direction (minimum of 15 km) for high resolution where ray coverage is good, and uniform spacing in both the y-direction (80 km) and z-direction (10 km). To test robustness (see Text S1 of the auxiliary material), we analyse the model resolution matrix (Figure S2 of the auxiliary material), perform bootstrap event resampling (Figure S3 of the auxiliary material) and also run synthetic recovery tests (Figures S4 and S5 of the auxiliary material) to investigate the resolving capabilities of our data and model set-up.

3. Results of 3D Tomographic Inversion

[7] Figure 2a shows the 3D P-wave velocity structure and relocated aftershock seismicity on four cross-sections oriented perpendicular to the regional trench axis. We observe all the primary structures identified in the 3D velocity model obtained for south-central Chile [*Haberland et al.*, 2009], (Figure S6 of the auxiliary material). We describe prominent features in the model (hereafter letters refer to those of Figure 2a). The continental crust of the South American plate (a) ($6.0 \geq v_p \geq 6.8$ km/s), the top of which has two low-velocity areas ($v_p < 6.0$ km/s) constituting the marine forearc (b) and the Central valley basin (c). The continental mantle (d) is characterised by a prominent upwelling with $v_p > 7.0$ km/s, ~200 km from the trench. The top of the downgoing oceanic crust (e), a dipping structure with $v_p \sim 6.8$ km/s is well defined by aftershocks. The interface velocity is similar to that inferred from other regional seismic studies [*Krawczyk et al.*, 2006; *Haberland et al.*, 2009].

[8] Section C-C′ traverses the mainshock nucleation region. Beneath the coastline, we observe a prominent, 40 km-wide, high v_p (>7 km/s) anomaly (f) with significant relief (up to 10 km). From a seismic refraction profile, *Krawczyk et al.* [2006] also infer a high v_p anomaly in this area, interpreting it as serpentinized mantle wedge material or mafic lower crustal rocks associated with late Paleozoic granitoid intrusions. We infer an elevated v_p/v_s ratio of 1.89 within the anomaly (Figure 2b). Accounting for our relocated seismicity distribution and previous estimates of slab interface geometry [*Haberland et al.*, 2009; *Hayes and Wald*, 2009], we define a regional thrust interface excluding the anomaly. The anomaly protrudes above the interface by around 5–10 km (Figure 2). By interpolating our v_p

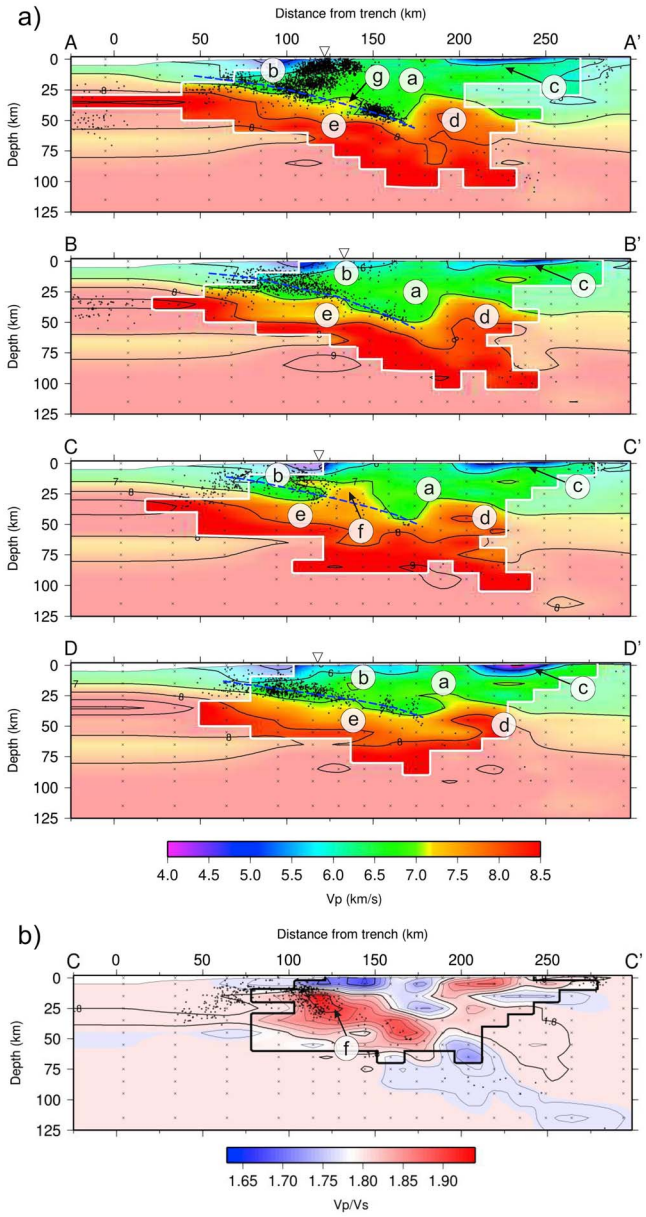

Figure 2. (a) Cross-sections through 3D P-wave velocity model. The location and orientation of each section is shown in Figure 1b. The coastline is given by black triangles. Features of the model are as interpreted as follows: (a) continental crust, (b) forearc basin, (c) central basin, (d) continental mantle, and (e) subducting oceanic crust. The blue dashed line is the unperturbed thrust interface. In section C-C′, (f) is a high-velocity anomaly located above the subducting interface, and (g) is a smaller high-velocity anomaly in the Pichilemu region (section A-A′). (b) Cross-section through v_p/v_s model along section C-C′. Black dots are relocated aftershocks with MI ≥ 3, with a minimum of 20 P- and 20 S-picks, respectively. The white lines denote the resolution limits, based on analysis of the resolution matrix (see Figure S2 and Text S1 of the auxiliary material).

model along the regional thrust interface (Figure 3), we find that the anomaly's maximum along-strike extent is 60 km. The nodal spacing used in the inversion may mean that the anomaly's height and along-strike extent may be exaggerated. From Section A-A′ (Figure 2a), we infer another, albeit smaller, high-velocity anomaly (g) in the Pichilemu region, ∼135 km from the trench, along the thrust interface (Figure 3).

4. Discussion

[9] The high v_p and v_p/v_s anomaly described above suggests that it is compositionally similar to hydrated oceanic crust [*Haberland et al.*, 2009] or mantle [*Carlson and Miller*, 2003]; therefore, it is of mafic origin, and must have once been subducted as part of the Nazca plate. From our tomographic images alone, we cannot resolve whether this structure represents a single seamount, an oceanic plateau, or a group of smaller seamounts. Furthermore, we cannot determine whether it remains attached to the subducting plate or was emplaced earlier in the overriding plate. We believe that this anomaly is not a residual igneous intrusion associated with the ancient magmatic arc: there is no correlation with surface outcrops of late Paleozoic – Triassic granitoids. Also, a high v_p/v_s ratio would not be indicative of a highly fractionated intrusion [*Christensen*, 1996; *Husen et al.*, 2000; *Reyners et al.*, 2006].

[10] Seismic evidence of subducted seamounts in a number of subduction zones is abundant [e.g. *Kodaira et al.*, 2002; *Husen et al.*, 2002; *Park et al.*, 2004]. However, it is important to constrain interpretations with additional geophysical evidence and to understand potential sources of heterogeneous topography on the subducting slab. We used the Earth Geopotential Model, EGM2008 [*Pavlis et al.*, 2008] to compute the regional Bouguer anomaly, subtracting the gravity effect of the subducting slab as contained in a regional 3D density model [*Tassara and Echaurren*, 2012]. The resultant forearc residual gravity anomaly $\Delta g_{\text{forearc}}$, is due to lateral density variations above the interplate fault; it shows a strong spatial correlation with v_p along the megathrust (Figure 3b). In particular, the anomalously high v_p region eastward from the hypocentre coincides with a prominent gravity high ($\Delta g_{\text{forearc}} > -70$ mGal), reinforcing our interpretation that the anomaly represents a dense mafic body located on top of the subducted slab. A smaller high v_p anomaly below the coast near 34.5°S (g) also correlates with a gravity high. We note that there is no correlation with high v_p for the positive gravity anomaly in the vicinity of the Arauco peninsula (∼37.4°S); this is further evidenced by the velocity model of *Haberland et al.* [2009]. We therefore believe that beneath the Arauco peninsula, although there may be an anomalous upper crustal density anomaly, it may not have a seismic velocity contrast with the normal continental crust.

[11] Westerly-dipping normal faults are observed in the marine forearc [*Geersen et al.*, 2011], WSW of the identified anomaly. Sedimentary underplating along the interface and subsequent gravitational collapse has been postulated to explain the presence of these faults, which are unusual along the central Chilean margin. Analogue models demonstrate that extensional faults can form in the wake of a subducting seamount due to enhanced sedimentary underplating [*Dominguez et al.*, 2000]; it is therefore feasible that a topographic high was once subducted in this region. Although no bathymetric high is observed offshore of the rupture region today, there is evidence for past subduction of a topographic anomaly related to the onset of contractional

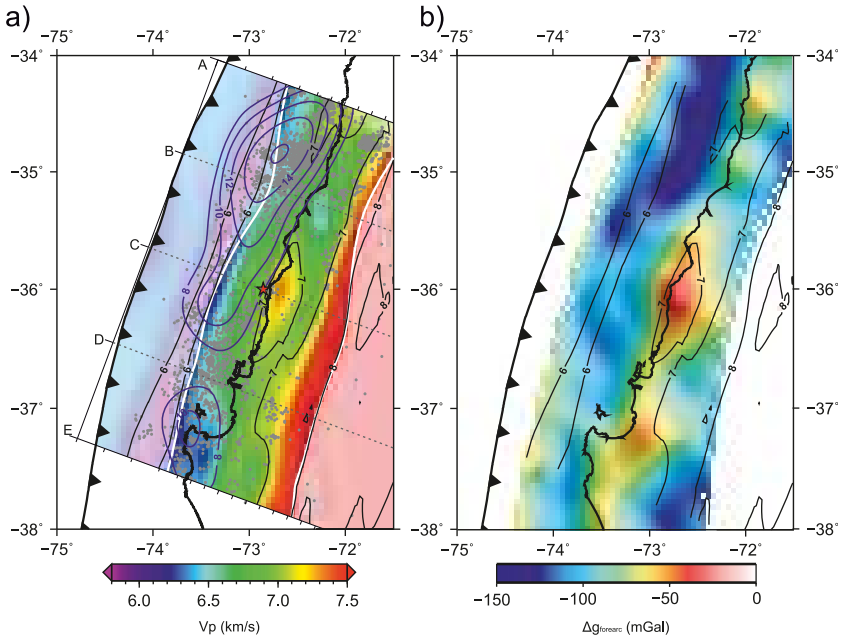

Figure 3. (a) Comparison of v_p along the plate interface (coloured image, black contours) with the co-seismic slip distribution of *Moreno et al.* [2012] (blue contours). The location of the high-velocity anomaly beneath the coastline correlates with a region of relatively co-seismic low slip. The two main slip patches correlate with lower P-wave velocities along the interface. Locations of events (grey circles) which lie along or close to the thrust interface are shown, highlighting the sparse seismicity associated with the anomaly. The red star is the NEIC epicentre, corrected by our 3D velocity model (see Text S2 and Figure S8 of the auxiliary material). The white line denotes the up- and down-dip resolution limits. (b) Forearc Bouguer gravity contribution, derived from the model of *Tassara and Echaurren* [2012]. Black lines are the v_p contours from Figure 3a for comparison.

deformation along the forearc at 3.6 Ma [*Folguera and Ramos*, 2009]. Ocean magnetic anomalies suggest that the point of intersection between the Mocha Fracture Zone (MFZ) and the Chilean trench would have been located in the Darwin gap, some 130 km north of its present position. The contemporary MFZ is associated with an abundance of seamounts. A detailed tectonic reconstruction of the Nazca plate could reveal more about the source of the subducted structure; in particular, if it was formed at the spreading ridge, then it may have a conjugate on the Pacific plate. It is worth noting that a simple tectonic reconstruction [*Müller et al.*, 2008] reveals that the formation region of the Nazca plate, now located along the central Chilean margin may have formed at a similar time to a zone of bathymetric

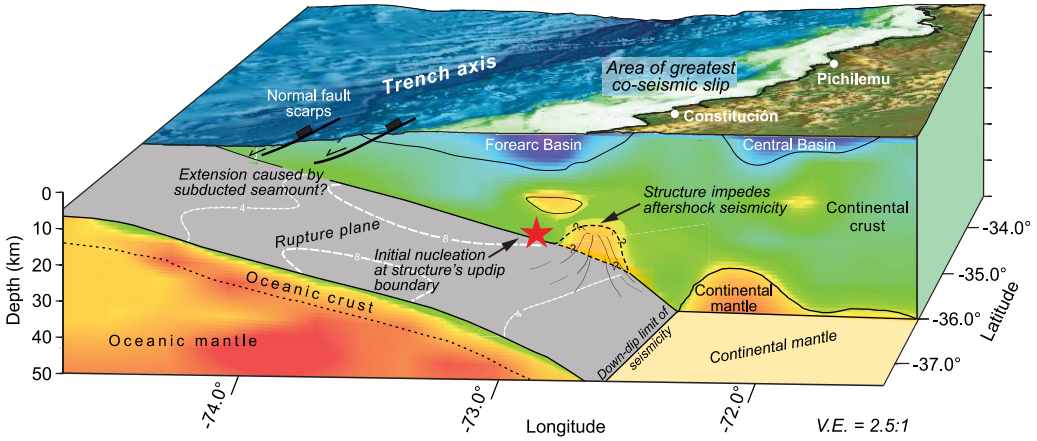

Figure 4. Schematic interpretative figure based on our tomographic model. Our 3D model is cut along two sections: 37.5°S to show the velocity structure of the oceanic lithosphere, and 36°S to show the structure of the forearc. The geometry of the rupture plane is illustrated between these two sections. The subducted topographic anomaly which lies beneath the coastal ranges at around 36°S disrupts the regular megathrust interface; however, we cannot tell whether it is still fully coupled to the downgoing plate. The red star denotes the mainshock's hypocentre. White lines along the interface show the co-seismic slip distribution [*Moreno et al.*, 2012].

heterogeneity, now located on the Pacific plate at 35°S (Figure S9 of the auxiliary material). Assuming that the structure is fully coupled to the downgoing plate and that the subduction rate has remained constant throughout its descent, it would have entered the trench at ~1.8 Ma.

[12] The topographic high in the Darwin gap is coincident with high pre-seismic locking (Figure S10 of the auxiliary material) [*Moreno et al.*, 2010; *Métois et al.*, 2012], small co-seismic slip, the location of the mainshock's hypocentre and reduced aftershock activity (Figure 3), suggesting that it influenced the rupture dynamics of the Maule earthquake. If the structure remains fully attached to the Nazca plate, then it likely influenced the rupture by acting as a geometric irregularity on the plate interface. We would expect associated active deformation within the forearc, a signal of which may be evident at the surface. Such topographic features on the plate interface have been shown to act as either asperities [*Husen et al.*, 2002] or barriers [*Kodaira et al.*, 2002]. One theory states that high relief on the downgoing plate increases coupling, thereby generating large earthquakes [*Scholz and Small*, 1997]. Conversely, damage sustained by the overriding plate as a seamount subducts may favour aseismic creep and small earthquakes, inhibiting the propagation of large ruptures [*Wang and Bilek*, 2011]. Due to the proximity of the subducted feature to the mainshock hypocentre, our results imply that high relief on the downgoing plate increases interface coupling and initiates large ruptures. The largest slip, however, was away from the anomaly, suggesting that its heterogeneous structure and stress conditions hinder the development of large co-seismic slip. The complex network of fractures expected within a subducted seamount [*Wang and Bilek*, 2011] may contribute to the low slip in this area, despite high interseismic coupling.

[13] Alternatively, if the topographic feature is now partially or wholly detached from the downgoing plate, or even accreted into the lower forearc crust, it could still disrupt normal seismogenesis along the interface. The sparse aftershock seismicity occurring within the region of anomalously fast material (Figures 2 and 3) would then indicate that this part of the interface is where fault slip is predominantly aseismic. In this case, the structure's updip boundary represents a transition between the locked and creeping zone, conducive to small seismic events [*Lapusta and Rice*, 2003]. It is plausible that a small event contributed to the nucleation of the 2010 Maule earthquake. Regardless of the current state of the observed structure, it appears to have influenced the rupture's initiation. Moreover, our model shows that in regions of large co-seismic slip, the megathrust is characterised by lower seismic velocities (Figure 3).

5. Conclusions

[14] Our model (Figure 4) shows that in the Darwin gap, a subducted topographic high, possibly a former seamount, played a part in both nucleating the earthquake and modulating the co-seismic slip once the rupture started. This dual behaviour of a subducted oceanic structure is a unique inference. High stress accumulation at its updip boundary is likely responsible for nucleating the initial rupture. Two end-member scenarios may represent the state of stress of the subducted structure. If it is sheared off from the downgoing plate, it may be continually creeping. Conversely, if it remains fully coupled to the downgoing lithosphere, it could be locked. In the latter case, the slip deficit accumulated since 1835 would be equivalent to a M_w 8.0 earthquake. These scenarios could potentially be resolved from analysis of active vertical tectonics on the surface, and subsequent models of deformation in the overriding plate. Our model shows that variations in seismic properties along the megathrust are important in controlling rupture dynamics of large earthquakes. We stress the need for further analyses of long-term afterslip and locking models to resolve the frictional characteristics of the Darwin gap seamount. Furthermore, it is essential to locate and understand such subducted topographic features in unbroken seismic gaps around the globe in order to better constrain their effect on interseismic locking and slip during large earthquakes.

[15] **Acknowledgments.** We thank IRIS, CNRS-INSU, GFZ, and Caltech for making continuous waveform data available. The complete IMAD data set can be accessed through the IRIS and GFZ data centers (http://www.iris.edu/dms/dmc/, http://webdc.eu/). Support in the field was given by the Seismological Service National of Chile, the Universidad of Concepción, and the University de Santiago de Chile. We are grateful to all field crews from partner organizations who participated in the deployment; without this combined effort, we would not have such a large and comprehensive data set. In support of this deployment we received funding from NERC (grant NE/I005420/1). Seismic instruments were provided by CNRS-INSU, IRIS/PASSCAL, GIPP(GFZ), GEF/SEIS-UK. We are grateful to two anonymous reviewers for providing insightful comments and suggestions, which have improved the manuscript. S.P.H. is funded by a NERC studentship. A.T. acknowledges support of Fondecyt project 1101034. We thank Kay Lancaster for assistance with producing Figure 4.

[16] The Editor thanks two anonymous reviewers for their assistance in evaluating this paper.

References

Carlson, R. L., and D. J. Miller (2003), Mantle wedge water contents estimated from seismic velocities in partially serpentinized peridotites, *Geophys. Res. Lett.*, *30*(5), 1250, doi:10.1029/2002GL016600.

Christensen, N. I. (1996), Poisson's ratio and crustal seismology, *J. Geophys. Res.*, *101*, 3139–3156, doi:10.1029/95JB03446.

Dominguez, S., J. Malavieille, and S. E. Lallemand (2000), Deformation of accretionary wedges in response to seamount subduction: Insights from sandbox experiments, *Tectonics*, *19*, 182–196, doi:10.1029/1999TC900055.

Folguera, A., and V. A. Ramos (2009), Collision of the Mocha fracture zone and a <4 Ma old wave of orogenic uplift in the Andes (36°–38°S), *Lithosphere*, *1*, 364–369, doi:10.1130/L66.1.

Geersen, J., et al. (2011), Active tectonics of the South Chilean marine fore arc (35°S–40°S), *Tectonics*, *30*, TC3006, doi:10.1029/2010TC002777.

Haberland, C., A. Rietbrock, D. Lange, K. Bataille, and T. Dahm (2009), Structure of the seismogenic zone of the southcentral Chilean margin revealed by local earthquake travel-time tomography, *J. Geophys. Res.*, *114*, B01317, doi:10.1029/2008JB005802.

Hayes, G. P., and D. J. Wald (2009), Developing framework to constrain the geometry of the seismic rupture plane on subduction interfaces a priori: A probabilistic approach, *Geophys. J. Int.*, *176*, 951–964, doi:10.1111/j.1365-246X.2008.04035.x.

Husen, S., E. Kissling, and E. R. Flueh (2000), Local earthquake tomography of shallow subduction in north Chile: A combined onshore and offshore study, *J. Geophys. Res.*, *105*(B12), 28,183–28,198.

Husen, S., E. Kissling, and R. Quintero (2002), Tomographic evidence for a subducted seamount beneath the Gulf of Nicoya, Costa Rica: The cause of the 1990 Mw = 7.0 Gulf of Nicoya earthquake, *Geophys. Res. Lett.*, *29*(8), 1238, doi:10.1029/2001GL014045.

Kissling, E., W. L. Ellsworth, D. Eberhart-Phillips, and U. Kradolfer (1994), Initial reference models in local earthquake tomography, *J. Geophys. Res.*, *99*, 19,635–19,646, doi:10.1029/93JB03138.

Kodaira, S., N. Takahashi, A. Nakanishi, S. Miura, and Y. Kaneda (2002), Subducted seamount imaged in the rupture zone of the 1946 Nankaido earthquake, *Science*, *289*, 104–106, doi:10.1126/science.289.5476.104.

Krawczyk, C. M., et al. (2006), Geophysical signatures and active tectonics at the south-central Chilean margin, in *The Andes: Active Subduction Orogeny*, edited by O. Oncken et al., pp. 171–192, Springer, New York.

Lange, D., et al. (2012), Aftershock seismicity of the 27 February 2010 Mw8.8 Maule earthquake rupture zone, *Earth Planet. Sci. Lett.*, *317–318*, 413–425, doi:10.1016/j.epsl.2011.11.034.

Lapusta, N., and J. R. Rice (2003), Nucleation and early seismic propagation of small and large events in a crustal earthquake model, *J. Geophys. Res.*, *108*(B4), 2205, doi:10.1029/2001JB000793.

Lay, T., and H. Kanamori (1981), An asperity model of great earthquake sequences, in *Earthquake Prediction: An International Review*, *Maurice Ewing Ser.*, vol. 4, edited by W. Simpson and G. Richards, pp. 579–592, AGU, Washington, D. C.

Lay, T., et al. (2010), Teleseismic inversion for rupture process of the 27 February 2010 Chile (Mw 8.8) earthquake, *Geophys. Res. Lett.*, *37*, L13301, doi:10.1029/2010GL043379.

Lorito, S., et al. (2011), Limited overlap between the seismic gap and coseismic slip of the great 2010 Chile earthquake, *Nat. Geosci.*, *4*, 173–177, doi:10.1038/ngeo1073.

Métois, M., A. Socquet, and C. Vigny (2012), Interseismic coupling, segmentation and mechanical behavior of the central Chile subduction zone, *J. Geophys. Res.*, *117*, B03406, doi:10.1029/2011JB008736.

Michael, A. J., and D. Eberhart-Phillips (1991), Relations among fault behaviour, subsurface geology, and three-dimensional velocity models, *Science*, *253*, 651–654, doi:10.1126/science.253.5020.651.

Moreno, M., M. Rosenau, and O. Oncken (2010), Maule earthquake slip correlates with pre-seismic locking of Andean subduction zone, *Nature*, *467*, 198–202, doi:10.1038/nature09349.

Moreno, M., et al. (2012), Toward understanding tectonic control on the M_w 8.8 2010 Maule Chile earthquake, *Earth Planet. Sci. Lett.*, *321–322*, 152–165, doi:10.1016/j.epsl.2012.01.006.

Müller, R. D., M. Sdrolias, C. Gaina, and W. R. Roest (2008), Age, spreading rates and spreading asymmetry of the world's ocean crust, *Geochem. Geophys. Geosyst.*, *9*, Q04006, doi:10.1029/2007GC001743.

Nippress, S. E. J., A. Rietbrock, and A. E. Heath (2009), Optimized automatic pickers: application to the ANCORP data set, *Geophys. J. Int.*, *181*, 911–925, doi:10.1111/j.1365-246X.2010.04531.x.

Okada, T., et al. (2007), Imaging the source area of the 1995 southern Hyogo (Kobe) earthquake (M7.3) using double-difference tomography, *Earth Planet. Sci. Lett.*, *253*, 143–150, doi:10.1016/j.epsl.2006.10.022.

Park, J. O., G. F. Moore, T. Tsuru, S. Kodaira, and Y. Kaneda (2004), A subducted oceanic ridge influencing the Nankai megathrust earthquake rupture, *Earth Planet. Sci. Lett.*, *217*, 77–84, doi:10.1016/S0012-821X(03)00553-3.

Pavlis, N., S. Holmes, S. Kenyon, and J. Factor (2008), An Earth gravitational model to degree 2160, *Geophys. Res. Abstr.*, *10*, EGM2008.

Reyners, M., D. Eberhart-Phillips, G. Stuart, and Y. Nishimura (2006), Imaging subduction from the trench to 300 km depth beneath the central North Island, New Zealand, with Vp and Vp/Vs, *Geophys. J. Int.*, *165*, 565–583, doi:10.1111/j.1365-246X.2006.02897.x.

Rietbrock, A., et al. (2012), Aftershock seismicity of the 2010 Maule Mw = 8.8, Chile, earthquake: Correlation between co-seismic slip models and aftershock distribution?, *Geophys. Res. Lett.*, *39*, L08310, doi:10.1029/2012GL051308.

Robinson, D. P., S. Das, and A. B. Watts (2006), Earthquake rupture stalled by a subducting fracture zone, *Science*, *312*, 1203–1205, doi:10.1126/science.1125771.

Ruegg, J. C., et al. (2009), Interseismic strain accumulation measured by GPS in the seismic gap between Constitución and Concepción in Chile, *Phys. Earth Planet. Inter.*, *175*, 78–85, doi:10.1016/j.pepi.2008.02.015.

Scholz, C. H., and C. Small (1997), The effect of seamount subduction on seismic coupling, *Geology*, *25*, 487–490, doi:10.1130/0091-7613(1997)025<0487:TEOSSO>2.3.CO;2.

Tassara, A., and A. Echaurren (2012), Anatomy of the Andean subduction zone: Three-dimensional density model upgraded and compared against global-scale models, *Geophys. J. Int.*, *189*, 161–168, doi:10.1111/j.1365-246X.2012.05397.x.

Thurber, C. H. (1983), Earthquake locations and three-dimensional crustal structure in the Coyote Lake area, central California, *J. Geophys. Res.*, *88*, 8226–8236, doi:10.1029/JB088iB10p08226.

Vigny, C., et al. (2011), The 2010 Mw 8.8 Maule megathrust earthquake of Central Chile, monitored by GPS, *Science*, *332*, 1417–1421, doi:10.1126/science.1204132.

Wang, K., and S. L. Bilek (2011), Do subducting seamounts generate or stop large earthquakes?, *Geology*, *39*, 819–822, doi:10.1130/G31856.1.